Progress in studying scintillator proportionality: Phenomenological model

G. Bizarri, N.J. Cherepy, W.S. Choong, *Member, IEEE,* G.Hull, W.W. Moses, *Fellow, IEEE,*, S.A. Payne, J. Singh, J.D. Valentine, *Senior Member, IEEE,*, A.N. Vasilev, and R.T. Williams

***Abstract*—We present a model to describe the origin of non-proportional dependence of scintillator light yield on the energy of an ionizing particle. The non-proportionality is discussed in terms of energy relaxation channels and their linear and non linear dependences on the deposited energy. In this approach, the scintillation response is described as a function of the deposited energy deposition and the kinetic rates of each relaxation channel. This mathematical framework allows both a qualitative interpretation and a quantitative fitting representation of scintillation non-proportionality response as function of kinetic rates. This method was successfully applied to thallium doped sodium iodide measured with SLYNCI, a new facility using the Compton coincidence technique. Finally, attention is given to the physical meaning of the dominant relaxation channels, and to the potential causes responsible for the scintillation non-proportionality. We find that thallium doped sodium iodide behaves as if non-proportionality is due to competition between radiative recombinations and non-radiative Auger processes.**

***Index Terms*—Scintillator, Proportionality, Scintillation mechanism, NaI:Tl, Density, Auger process**

I. Introduction

Inorganic scintillators were widely studied within the past half century, driven to a large degree by the needs in areas such as medical imaging, high energy physics, security inspection, and monitoring systems. This led to the discovery of many new scintillator materials [1][2] and to a better understanding of the physical processes governing the transformation of ionizing radiation into scintillation light [3][4].

Nonetheless some issues still need to be solved. One of the major challenges for the scintillation community is to push the limits of energy resolution downward. The energy resolution of scintillators is for some reason poorer than one expects on statistical grounds [5]. This significant degradation is mainly due to the non-proportionality response of scintillators to ionization radiation [6][7]. At present, the origin of non-proportionality is not clearly understood and it is not possible to select materials for which non-proportionality effects can be estimated a priori.

In this paper, a phenomenological model is presented to study qualitatively and quantitatively the proportionality response of scintillator materials. The model is discussed in terms of energy relaxation channels and their linear and non linear dependences on the deposited energy. Based on this model, the electron response of thallium doped sodium iodide is analyzed. The data together with the model provide us with insight of the potential causes of NaI:Tl non-proportionality.

II. Phenomenological model

In first approximation, two main characteristic shapes are observed in scintillator non proportionality response:

- Type 1: The scintillation response curve is nearly constant at high excitation energy and decreases with decreasing excitation energies (Fig. 1). This kind of response is the most common case. Oxides, lanthanum halides, and intrinsic undoped scintillators exhibit this type 1 behavior.
- Type 2: The scintillation response curve shows a maximum for intermediate excitation energies and a decrease with increasing and decreasing excitation energies (Fig. 1). This kind of response is typical for doped alkali halides.

Our approach is aimed at describing and explaining the origin of Type 1 and Type 2 non proportionality response. It is articulated around a model that includes two main processes: the track creation and scintillation mechanisms and that allows us to simulate the proportionality response of materials.

A. Track model

In a scintillator, the track created by a high energy particle is complex and depends on numerous parameters such as energy and type of particle, lattice... A complete and rigorous model describing the process is outside the boundaries of this article. In our approach, we use the time and space dependence of the deposited energy density, $\eta(\overrightarrow{r},t)$ to model the track. From the calculation of $\eta(\overrightarrow{r},t)$, one can extrapolate the density of energy carriers, $n(\overrightarrow{r},t)$ also defined for any position along the track, $\overrightarrow{r}$ and at any time, t, after the absorption of the initial particle. Note that this carrier density $n_i(\overrightarrow{r},t)$ is just the energy density $\eta(\overrightarrow{r},t)$ divided by a constant (the energy needed to create a carrier). The track is assumed to be unaffected by any

This work was supported by the Domestic Nuclear Detection Office in the Department of Homeland Security and by the National Nuclear Security Administration, Office of Defense Nuclear Nonproliferation, Office of Nonproliferation Research and Development (NA-22) of the U.S. Department of Energy under Contract No. DE-AC02-05CH 11231.

G. Bizarri, W.S Choong, W.W. Moses are with Lawrence Berkeley National Laboratory, Berkeley, CA 94720, USA (telephone: +1-510-495-2944, e-mail: gabizarri@lbl.gov).

N.J. Cherepy, G.Hull, S.A. Payne, J.D. Valentine are with Lawrence Livermore National Laboratory, Livermore, CA 94551, USA.

J. Singh is with Faculty of Education, Health and Science, Charles Darwin University, Darwin, NT 0909, Australia.

A.N. Vasilev is with Institute of Nuclear Physics, Moscow State University, Moscow, 119991, Russia.

R.T. Williams is with Department of Physics, Wake Forest University, Winston-Salem, NC 27109, USA.

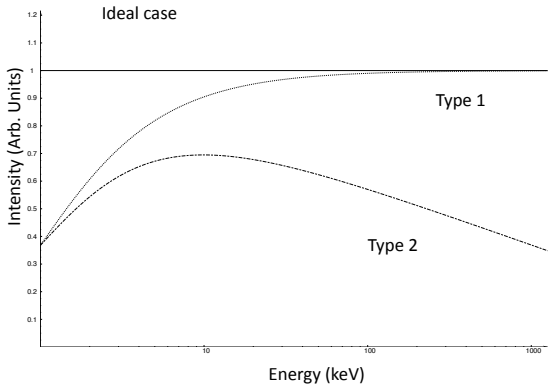

Fig. 1. Common electron response for scintillators as a function of the incident energy

changes in particle direction and has a cylindrical shape (radius ρ). n($\overrightarrow{r}$,t=0) is determined from the linear deposited energy density $\frac{dE}{dx}$, the energy to create an excitation $E_{excitation}$ and the radius of the track ρ. $E_{excitation}$ is assumed to be equal to βE_{gap} with β a constant between 2 and 3 and E_{gap} the energy gap of the scintillator [8]:

$$\begin{aligned} n(\overrightarrow{r}, t=0) &= \frac{\eta(\overrightarrow{r},t=0)}{E_{excitation}} \\ &= \frac{-\frac{dE}{dx}|_{\overrightarrow{r}}}{\pi\rho^2 E_{excitation}} = \frac{-\frac{dE}{dx}|_{\overrightarrow{r}}}{\pi\rho^2\beta E_{gap}} \end{aligned} \quad (1)$$

with $\overrightarrow{r}$ defined as $\overrightarrow{r}_{longitudinal}$ along the track and $\overrightarrow{r}_{transversal}$ along the radius of the track. In the hypothesis of a cylindrical track, $n(\overrightarrow{r}, t=0)$ is calculated for $\overrightarrow{r}_{transversal}$ less than ρ. For $\overrightarrow{r}_{transversal}$ higher than ρ, $n(\overrightarrow{r}, t=0)$ is equal to 0 (Fig. 2).

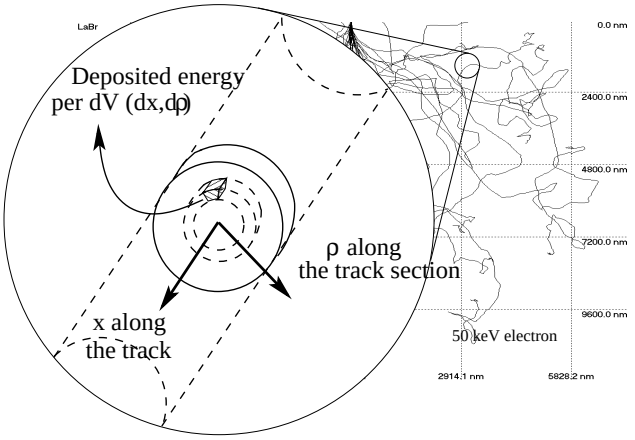

Fig. 2. Scheme of track created by an electron [9]. The expended area shows the track section.

The energy gap of materials is known from literature and the radius of the track can be estimated from the mean free path of low energy electrons (typically nanometer scale for electrons with an energy between 10 and 100 eV - Fig. 3 and discussion below). The linear deposited energy has to be calculated.

In order to obtain the electron stopping power over a large range of energy (from about 10 eV to 1 MeV), we need to use a different approach than the analytical calculation of $\frac{dE}{dx}$ with the familiar Bethe-Bloch formula, which is valid only for energies higher than 10 keV. To do so, one can employ many approaches which include calculations of energy loss function that rely on a number of approximations (see, e.g.,[10 - 15]). We use a modified form of these approximations, which helps us to estimate the stopping power in a wide energy range from several eV to 1 MeV (for energies below electron-positron creation threshold). The energy losses can be described in polarization approximation as:

$$-\frac{dE}{dx} = \frac{2}{\pi a_B m v^2}\int_0^E \hbar\omega\, d(\hbar\omega)\int_{q_-}^{q_+}\frac{dq}{q} Im(-\frac{1}{\epsilon(\omega,q)}) \quad (1)$$

where $\hbar q_+$ and $\hbar q_-$ are the maximal and minimal momentum transfer, respectively. For the relativistic case:

$$\begin{aligned} \frac{mv^2}{2} &= E\frac{2+\frac{E}{mc^2}}{2(1+\frac{E}{mc^2})} \\ \hbar q_\pm &= p(E) \pm p(E-\hbar\omega) \\ &= \frac{\sqrt{(E+mc^2)^2-m^2c^4}\pm\sqrt{(E-\hbar\omega+mc^2)^2-m^2c^4}}{c} \\ &= \sqrt{E(E+2mc^2)} \pm \sqrt{(E-\hbar\omega)\,(E-\hbar\omega+2mc^2)} \end{aligned}$$

The exchange of indistinguishable electrons is not included in this form of the stopping power. However this effect modifies the stopping power only when the energy of the secondary electron and scattered primary electron are about the same, i.e. the exchange modifies mainly the low-energy part of the stopping power (below mean ionization energy), and the decrease is no more than a factor of two.

We will use the approximation when the q-dependence of dielectric permittivity is neglected: $Im(-\epsilon^{-1}(\omega,q)) \approx Im(-\epsilon^{-1}(\omega,0))$. In this case we neglect the effects connected with the Bethe ridge (see, e.g., [10]), i.e. large-angle scattering on quasi-free electrons which slightly overestimates the stopping power. This approximation is equivalent to using the Optical Oscillator Strength (OOS) approximation instead of the Generalized Oscillator Strength (GOS) approximation (see, e.g., [10][11]).

The dielectric permittivity $\epsilon(\omega,0)$ is calculated using the Evaluated Photon Data Library (EPDL97) data bases developed at Lawrence Livermore National Laboratory. We apply these data bases mainly for ionic crystals. In this case we use the following corrections: (1) we modify the ionization energies of elements using the rigid shift of core level positions in order to obtain the correct ionization energies of shallow shells (a way to account for Madelung crystal potential), and (2) we change the population of the outer shells (e.g. for NaI we use the pure ionic model Na^+I^- with 6 electrons at 5p iodine valence shell and zero electrons at 3s sodium shell). The partial photon absorption cross-sections from EPDL97 library are summed in order to obtain the imaginary part of dielectric permittivity $\epsilon_2(\omega,0)$. The real part of this function $\epsilon_1(\omega,0)$

is reconstructed using the Kramers-Krönig procedure. Both $\epsilon_2(\omega,0)$ and $Im(-\epsilon^{-1}(\omega,0))$ functions are checked using the sum rules for the total number of electrons per unit crystal cell and for the value of low-frequency dielectric permittivity. Therefore we verify that the resulting energy loss function shows the plasmon peak at the correct energies, and that the intensity of this peak is also realistic. Then the stopping power is calculated using the formula:

$$-\frac{dE}{dx} = \frac{1}{\pi a_B E}\frac{2+\frac{E}{mc^2}}{2(1+\frac{E}{mc^2})}\int_0^E \hbar\omega\, d(\hbar\omega) Im(-\frac{1}{\epsilon(\omega,0)}) \\ ln\frac{\sqrt{E}\sqrt{E+2mc^2}+\sqrt{E-\hbar\omega}\sqrt{E+2mc^2-\hbar\omega}}{\sqrt{E}\sqrt{E+2mc^2}\sqrt{E-\hbar\omega}\sqrt{E+2mc^2-\hbar\omega}} \quad (2)$$

Fig.4 and 3 present $\frac{dE}{dx}$ and Mean Free Path as a function of the electron energy calculated for a NaI crystal.

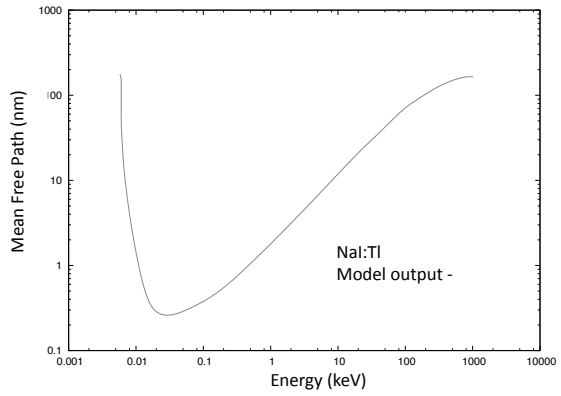

Fig. 3. Mean Free Path as a function of the incident electron energy calculated for NaI:Tl

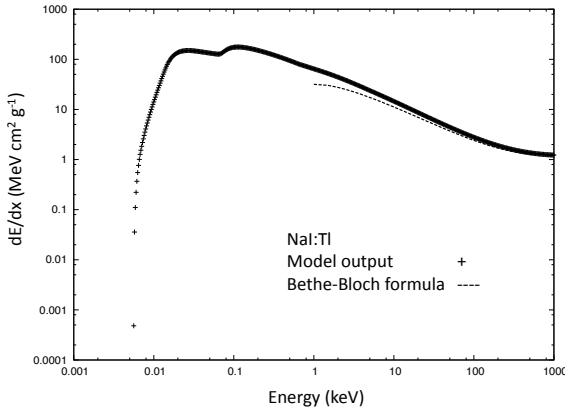

Fig. 4. Deposited energy density $\frac{dE}{dx}$ as a function of the incident electron energy calculated for NaI:Tl

B. Scintillation mechanism

After the track creation, the energy of the initial particle is assumed to be converted into energy carriers such as excitons, electron-hole pairs, and self-trapped excitons. The density of each type of energy carrier at t=0, $n_i(\overrightarrow{r},t=0)$ is calculated from Eq. 1 and a branching ratio between the different energy carrier types. The evaluation of the branching ratio is estimated from optical, scintillation data. Each of these energy carriers can undergo transport, trapping, transfer and/or relaxation mechanisms.

The model proposed is a statement that the time dependent density of each type of energy carrier, $n_i(\overrightarrow{r},t)$ can be expressed for each point along the track by a simple ordinary differential equation. $n_i(\overrightarrow{r},t)$ is governed by a rate equation that contains both radiative and non-radiative terms. Each kinetic rate depends linearly or non-linearly on the density of each type of energy carrier. Upon solving this differential equation, one then has the density of each type of energy carrier as a function of time. Integrating over time gives the total light yield output for one infinitesimal track volume, and integrating over the track gives the light yield. This assumption assumes that the scintillation mechanism is not affected by the migration of the energy carriers. The assumption is valid for modern and commercial scintillators where the energy carriers relax very efficiently on emitting centers. This implies also that the migration of carriers from one part of the track to another is not included in the model.

More specifically, for one energy carrier the following equation applies:

$$-\frac{dn_i(\overrightarrow{r},t)}{dt} = \sum_j A_j^i n_i(\overrightarrow{r},t)^j \\ + \sum_j \left\{ \sum_{k\neq i} G_j^{i\to k}\, n_i(\overrightarrow{r},t)^j - G_j^{k\to i}\, n_k(\overrightarrow{r},t)^j \right\} \quad (3)$$

where i and k are different energy carrier types (e.g. exciton and electron). $n_i(\overrightarrow{r},t)$ is the time dependent density of the i^{th} energy carrier type at one point along the track. A_j^i are the scintillation mechanism kinetic rates for the i^{th} energy carrier type. Each A_j^i is related to a different scintillation mechanism with a dependence on $n_i(\overrightarrow{r},t)$ to the power of j. A_j^i can correspond to an emission or a quenching mechanism, R_j^i and K_j^i, respectively. $G_j^{i\to k}$ are the transfer rates from the i^{th} to the k^{th} energy carrier type. As for A_j^i, each energy transfer mechanism has a dependence on $n_i(\overrightarrow{r},t)$ to the power of j. The initial conditions are determined from $n(\overrightarrow{r},0)$, the total deposited energy density at t = 0 and at each point along the track. The branching ratio between the different energy carriers gives the distribution of $n(\overrightarrow{r},0)$ over each energy carrier.

Solving the coupled differential equation system (Eq.3) gives each energy carrier density at one point along the track as a function of time, $n_i(\overrightarrow{r},t)$. From $n_i(\overrightarrow{r},t)$, one can determine the number of emitted photons per unit of volume at one position along the track for the i^{th} energy carrier type, $N_i^{photon}(\overrightarrow{r},t)$ (Fig.2):

$$N_i^{photon}(\overrightarrow{r},t) = \sum_{j=1}^{3} R_j^i\; n_i(\overrightarrow{r},t)^j \quad (4)$$

The total number of excitations per unit of volume at one position along the track for the ith energy carrier type, $N_i^{total}(\overrightarrow{r},t)$ is naturally given by $n_i(\overrightarrow{r},t)$.

The decay curve for one scintillation event of initial energy E_0 and for the ith energy carrier type, $N_i(t)|_{E_0}$, is given by the integration of $N_i^{photon}(\overrightarrow{r},t)$ over the track, normalized by the total number of charge for the i^{th} energy carrier, $N_i^{total}(\overrightarrow{r},t)$:

$$N_i(t)|_{E_0} = \frac{\int_{track}\ dV\ N_i^{photon}(\overrightarrow{r},t)}{\int_{track}\ dV\ N_i^{total}(\overrightarrow{r},t)} \tag{5}$$

The response for one scintillation event of initial energy E_0 and for the ith energy carrier type, $N_i|_{E_0}$ is derived from the same relation by integrating over time:

$$N_i|_{E_0} = \frac{\int_0^{\inf}\ dt\ \int_{track}\ dV\ N_i^{photon}(\overrightarrow{r},t)}{\int_0^{\inf}\ dt\ \int_{track}\ dV\ N_i^{total}(\overrightarrow{r},t)} \tag{6}$$

In this article, the limits for the time integration are from 0 to 1 ms. Compared to the time response of the scintillator, we chose this large time constant to integrate the totality of the light output. In forthcoming studies, we plan to compare the role of the integration interval on the electron response by tuning both experimental and modeled gate widths.

Finally, the decay curve and the response of a scintillator for an excitation E_0 is calculated by summing the decay curves and the response of each energy carrier:

$$N(t)|_{E_0} = \sum_i\ N_i(t)|_{E_0} \tag{7}$$

and

$$N|_{E_0} = \sum_i\ N_i|_{E_0} \tag{8}$$

The proportionality curve is constructed by repeating the calculation of $N|_{E_0}$ over a broad range of particle energy values.

C. Relation between model parameters and physical mechanisms

It is obvious that for simulating the total light yield, we need to know the rates of the various processes considered above in a scintillator. Although there are many parameters in this model, it turns out that only a few of the parameters controls the shapes of the non proportionality response curves and the placement along their energy scale. In most of the cases, the dependence of A_j^i rates can be restrained to linear, quadratic and cubic types (j = 1, 2 and 3). It is also important to note that all the parameters represent physically possible processes, as explained below

- Linear rates - A_1^i: The most common 1^{st}-order mechanisms are the radiative and non radiative decay of an emitting center, R_1 and K_1, respectively. There are numerous examples of those processes in scintillators. Excitonic emission and quenching via non-radiative multiphonon relaxation are typical examples. Another case of 1^{st}-order mechanism corresponds to energy transfers involving one donor and one acceptor, G_1, such as excitonic energy transfer to an activator ion (see for instance lanthanum halides scintillation mechanism [16]).
- Quadratic rates - A_2^i: 2^{nd}-order processes are well known in scintillators and occur when the emission involves the binary electron and hole capture at the luminescent ion, i.e. R_2 [17]. Less known are the mechanisms linked to a quadratic quenching of the energy, K_2, such as exciton-exciton collisions and resonant interactions of close excitations even if immobilized on activator ions [18]. In those cases, one excitation can make a transition to the ground state while exciting a nearby exciton to a high-lying state which decays non-radiatively back to the lowest excited state or to the ground state. The generic term for these mechanisms is Auger recombination whether radiative or not [19].
- Cubic rates - A_3^i: The experimental evidence of a 3^{rd}-order mechanism is found in semiconductors [20][21] and enhancing light emission device communities [22]. The mechanism corresponds to the quenching of the energy carriers (K_3) via the interaction of 3 particles, 2 electrons and 1 hole or 1 electron and 2 holes. The physical process is very similar to the one described previously for the exciton Auger decay. An electron and a hole recombine transferring their energy to the third particle. This particle loses its additional energy via thermalization and is trapped (non-radiative Auger de-excitation with trapped carriers).

Actually taken independently of each other, the above described linear, quadratic and cubic rates lead to a flat response as a function of the energy. It is the competition between the kinetic rates that is responsible of the shape of the proportionality response. If all the processes are potentially active in a scintillator, usually the number of parameters is limited to few constant rates. The set of parameters is determined according to the scintillation mechanism for each scintillator studied. On the contrary, a minimum of parameters is needed to reproduce and fit type 1 and type 2 non proportionality curves. This minimal number is discussed in the next paragraph.

III. Proportionality response: Qualitative approach

A. Simplified case

While equations 3-8 look formidable, in most cases only a few kinetic rates A_j^i and $G_j^{i\rightarrow k}$ are necessary to describe the non proportionality curve. Type 1 and type 2 responses (Fig. 1) can be reproduced by taking into account only the main energy carrier present in the scintillation mechanism ($n_i(\overrightarrow{r},t)\ \rightarrow\ n(\overrightarrow{r},t)$) and only three and four relaxation channels, respectively. Although this is definitely an oversimplification and ignores many processes, this approach is a first approximation study. It highlights the minimum and mandatory parameters to reproduce Type 1 and 2 curves and consider only one energy carrier type. For a more complete study, the number of energy carriers and parameters is dependent on the complexity of the scintillation mechanism and different for each material studied. Such study will be published later for specific materials.

- For Type 1 response: Linear emission and quenching (kinetic rates R_1 and K_1, respectively) and Quadratic emission (kinetic rates K_2). Eq.3 becomes:

$$-\frac{dn(\overrightarrow{r},t)}{dt} = (R_1 + K_1)n(\overrightarrow{r},t) + K_2 n(\overrightarrow{r},t)^2 \quad (9)$$

- For Type 2 response: Linear emission and quenching (kinetic rates R_1 and K_1, respectively) Quadratic quenching (kinetic rates R_2) and Cubic quenching (kinetic rate K_3). Eq.3 becomes:

$$-\frac{dn(\overrightarrow{r},t)}{dt} = (R_1 + K_1)n(\overrightarrow{r},t) + R_2 n(\overrightarrow{r},t)^2 + K_3 n(\overrightarrow{r},t)^3 \quad (10)$$

Non-proportionality Type 1 and Type 2 at low and high energy density can be understood by considering the local probability of emission, $\mathcal{P}$ and its asymptotic behavior as a function of the density of energy carriers (Table I and discussion here after).

For Type 1:

$\mathcal{P} = \frac{R_1}{R_1+K_1+K_2 n(\overrightarrow{r},t)}$

giving $\mathcal{P}|_{n\to\infty} \equiv \frac{R_1}{K_2 n(\overrightarrow{r},t)} \equiv 0$ and $\mathcal{P}|_{n\to 0} \equiv \frac{R_1}{R_1+K_1}$

For Type 2:

$\mathcal{P} = \frac{R_1+R_2 n(\overrightarrow{r},t)}{R_1+K_1+R_2 n(\overrightarrow{r},t)+K_3 n(\overrightarrow{r},t)^2}$

giving $\mathcal{P}|_{n\to\infty} \equiv \frac{R_2}{K_3 n(\overrightarrow{r},t)} \equiv 0$ and $\mathcal{P}|_{n\to 0} \equiv \frac{R_1}{R_1+K_1}$

For Type 1 response at high density of energy carrier, the local probability of emission $\mathcal{P}$ is dominated by the first order terms. $\frac{dE}{dx}$ (and so $n(\overrightarrow{r},t)$) is small for high energy particles. The response is governed by R_1 and K_1 that is independent of the initial energy of the particle. This part of the electron response curve is flat. With decreasing energy (increasing $\frac{dE}{dx}$ and so $n(\overrightarrow{r},t)$) the second order term K_2 becomes dominant. The light yield decreases. Below 5 keV, the curve reaches its asymptotic behavior corresponding to $\frac{R_1}{K_2 n(\overrightarrow{r},t)}$. At intermediate energy the response is governed by the competition between the linear and quadratic terms.

Type 2 response is also dominated by the first order terms at high density of excitation. The response is governed by R_1 and K_1. With decreasing energy (increasing $\frac{dE}{dx}$) the second order term R_2 becomes dominant. The light yield increases. When the third order term becomes of the same order as the second order emission the response presents a maximum, around 10 keV in Fig. 1. Below this maximum, the response undergoes a decrease of the relative light output due to the quenching mechanism K_3. In this energy range, the response follows an asymptotic behavior $\frac{R_2}{K_3 n(\overrightarrow{r},t)}$.

B. Application to thallium doped sodium iodide

In Fig. 5 the relative light yield for a NaI(Tl) crystal is reported as a function of the electron energy. The measurement was recorded with SLYNCI [23][24], a new facility using the Compton coincidence technique [25]. The data distribution is normalized at the energy value of 350 keV. The shape is characteristic of thallium doped alkali halide at room temperature. The response shows a maximum around 15 keV. Above 15 keV, the light yield decreases. The minimum value in our measured energy range is reached at 450 keV for a relative light output of 98,5% compared to the response recorded at 350 keV. Below 15 keV, the light output decreases continuously. The minimum value in our measured energy range is obtained at 3 keV and corresponds to 105% of the response recorded at 350 keV.

TABLE I
ASYMPTOTIC DEPENDENCE OF PROPORTIONALITY RESPONSE ON MODEL PARAMETERS

		Asymptotic behavior	
Response	Process	Small $n(\overrightarrow{r},t)$	High $n(\overrightarrow{r},t)$
Type 1	R1, K1	$\frac{R_1}{R_1+K_1}$	$\frac{R_1}{K_2 n(\overrightarrow{r},t)}$
	K2		
Type 2	R1, K1	$\frac{R_1}{R_1+K_1}$	$\frac{R_2}{K_3 n(\overrightarrow{r},t)}$
	R2		
	K3		

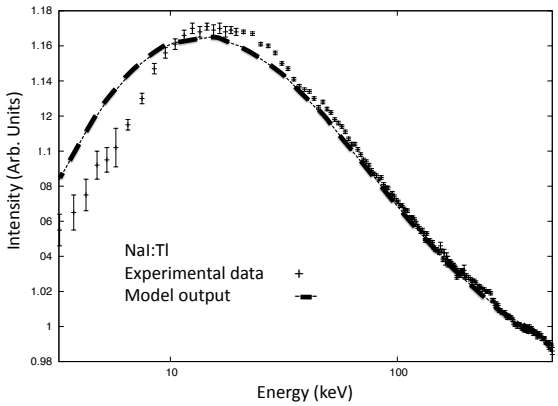

Fig. 5. NaI:Tl proportionality curve (dots) and fitting curve from the model (line)

As mentioned in the previous paragraph, the simplest model to reproduce this type of non proportionality response includes one differential equation with 4 kinetic rates, R_1, K_1, R_2 and K_3 (cf Eq. 10). To constrain our model we used x-ray excited decay curve to determine the value of R_1. The x-ray beam has mean energy of 19 keV for a pulse duration of about 40 ps fwhm [26]. Fig.6 shows the decay curve. As the shape of the decay curve presents a complex structure, includes a rise time and is not a simple exponential, the data are fitted using Eq.11 to estimate the intrinsic decay time ($\tau = \frac{1}{R_1}$) [27].

$$N(t) = \frac{A_1}{\tau} e^{-\frac{t}{\tau}} + \frac{A_2}{\tau - \tau_R}(e^{-\frac{t}{\tau}} - e^{-\frac{t}{\tau_R}}) \quad (11)$$

The fitting curve is shown on Fig.6. The values τ and τ_R extracted from the fitting procedure are 170 ns and 60 ns, respectively. τ gives a linear constant rate, R_1, of 5.9 10^6

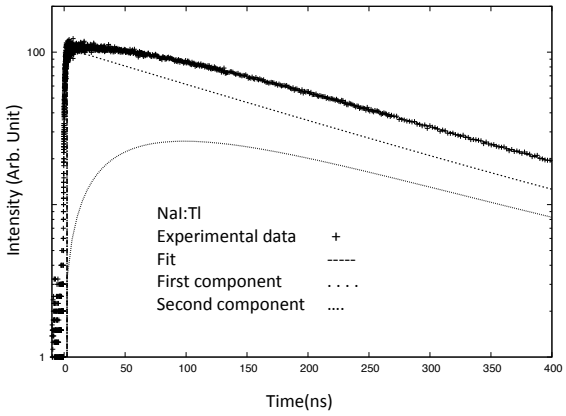

Fig. 6. X-ray excited decay curve of NaI:Tl recorded at room temperature (dots). The dotted line represents the fitting curve.

s^{-1}. The three other parameters, K_1, R_2 and K_3, are used as free input parameters allowing the model to fit NaI:Tl non-proportionality response.

C. Results

The proportionality response calculated from the model is presented in Fig.5. The result is in reasonable agreement with the data all over the energy range. Although our model includes only three free parameters, it reproduces the important qualitative features and trends of the electron response of NaI:Tl. The biggest discrepancy between the data and the model are found at low energy, below 10 keV, where the experimental error is the largest. In this energy range, the difference between the experimental and calculated response correspond to less than 5%.

Table II shows the parameters extracted from the fitting procedure of the model.

TABLE II
FITTING PARAMETERS FROM THE MODEL

Parameter	Process		Fitting
	Type	$\frac{dE}{dx}$ dependence	output
R_1	Emission	Linear	5.9 10^6 s^{-1} (experimental)
K_1	Quenching	Linear	4.2 10^6 s^{-1}
R_2	Emission	Quadratic	1.8 10^{-6} cm^3 s^{-1}
K_3	Quenching	Cubic	1.07 10^{-20} cm^6 s^{-1}

IV. Discussion

The aim of this paper is to develop a simple model yielding intuitive trends influenced by choices of a few identifiable physical parameters. This leads to a number of approximations in the treatment of the proportionality response. They are mainly linked to the simplicity of the model used to simulate the track creation and the validity of the scintillation mechanisms depending on the recombination rate equations. Both approximations are discussed in Section A.

Finally, an attempt to link the parameters extracted from the model to microscopic mechanisms is done. For the first time, the potential causes of non proportionality in NaI:Tl are discussed in Section B.

A. Validity of the model: Track and scintillation mechanisms

The validity of the track creation model has three main issues related to the use of $\frac{dE}{dx}$ as unique parameter:

- Validity at low electron energies
- q-dependence of electron scattering
- Electron exchange.

The calculation of $\frac{dE}{dx}$ over a large range of energy, from the band gap energy of the material to 1 MeV, is a major step in our model. The determination and validation of this calculation is easy at high energy but the extrapolation at low energy is not trivial. To validate it at high energy, the $\frac{dE}{dx}$ curve calculated with the relativistic Bethe-Bloch formula is plotted in Fig.4. The agreement between the two curves is excellent above 10 keV, the range of validity of the Bethe-Bloch formula. At low energy, below 100 eV, the lack of an analytic model to describe the linear energy density makes any direct comparison impossible. The validity of our model is estimated by comparing experimental data taken from electron energy loss spectroscopy literature giving the mean free path of low energy electrons with the value extrapolated from our $\frac{dE}{dx}$ calculation. The literature gives typical values between 1 and 10 nm for the mean free path of low energy electrons (see e.g., [13] [28]). These values are in good agreement with the ones extracted from our model, typically few nanometers (cf Fig. 3). Another issue in our model is the constraint assigned to the angular momentum transfer in scattering on quasi-free electrons, q. q is fixed to 0. We mentioned that this approximation leads to a slight overestimate of the deposited energy density. In addition, the lack of correction factor for electron exchange in our formula also tends to increase the $\frac{dE}{dx}$ values at low energy. The combined effect of these parameters overestimates $\frac{dE}{dx}$ below 100 eV. We evaluated the correction factor to be between 2 or 3 in this energy range compared to our calculation. The generalization of this formula to account for q-dependence of the dielectric permitivity and electron exchange will be presented elsewhere. By accounting for large-angle scattering, our track creation model will be strengthened by allowing a valid description of the track branching. This point is also valid for the delta rays creation during the track formation. This mechanism is not accounted for in our model, but is certainly present in the measured electron response. This process could be of importance to explain the discrepancy observed at low energy between the experimental data and the model output.

The use of a scintillation model that depends on concentration of excitation needs also some clarification. The main issue with this hypothesis is the definition of energy carrier density by itself. The density is well defined in the track and in the area surrounding of the track. The number of energy carriers per volume unit is high. The use of the density becomes more problematic when the number of excitations is small or when the volume that the charge carriers occupy

expands and becomes large. Our hypothesis is valid outside of these two extreme cases. It implies for the scintillation mechanism a transfer of the energy to the emitting centers or a trapping mechanism that is very efficient and occurs promptly after the track creation. In this hypothesis the use of density remains valid. In other terms the validity of our model is correct when the the scintillation mechanism is not governed by the migration of the charge carriers or when this migration mechanism is not the dominant process. This situation is usually the case at room temperature for common bright scintillators. At low temperature and for less efficient material, the validity of model should be checked.

B. Relation between model parameters and scintillation mechanism

We applied our minimalist model to the electron response of NaI:Tl in order to determine if it contained sufficient detail to be useful. Despite the simplicity of the model, it shows a good agreement with the experimental result and can be used as a first order to discuss the causes of non proportionality in NaI:Tl.

The necessity of having linear, quadratic and cubic kinetic rates in the model to reproduce the correct response of the scintillator may be understood by summarizing the scintillation properties of undoped and Tl doped NaI. The undoped compound presents an excitonic emission with a broad band centered around 300 nm [30][31]. This emission undergoes a strong thermal quenching with increasing temperature [32]. At low temperature, below 77 K, the light output is 76,000 ph per MeV while at room temperature very little light can be detected [33]. When thallium ions are added, the scintillation properties change. The emission becomes mainly due to the thallium ions and corresponds to a broad band centered around 420 nm [36]. The light output is stable at room temperature [32]. The recorded scintillation light output is of 38,000 ph per MeV at room temperature [33]. Moszynski et al. have studied the temperature dependence of NaI:Tl decay curve under gamma excitation [34][35]. They show a strong temperature dependence of the NaI:Tl response. Below 0^o C, the decay curve becomes complex with the presence of multi exponential decay components, mainly a fast and a slow component. At low temperatures i.e. below 270 K, the slow component contribution reaches 60% of the total light, while at an elevated temperature the initial slow decay was replaced by a delayed maximum and the slow component becomes insignificant.

Based on the scintillation properties of undoped and thallium doped sodium iodide, we propose that the observed kinetic rates can be assigned to the following physical processes:

- The linear emission mechanism (R_1) is the energy transfer from self trapped excitons to thallium ions.
- The linear quenching mechanism (K_1) is due to several mechanisms: the thermal quenching of the STE either due to configurational quenching or dissociation of STE and/or the trapping of an electron or hole on defects.
- The quadratic emission mechanism (R_2) is the sequential capture of an electron/hole pair at a thallium site.
- The cubic quenching mechanism (K_3) is attributed to non radiative Auger processes between two electrons and a hole.

These hypotheses are in qualitative agreement with the undoped and doped scintillation properties of NaI. At low temperature in the pure compound the STE thermal quenching is negligible. The emission is purely excitonic. When the temperature increases the energy loss due to the thermal quenching of the STE becomes dominant over the emission. With dopant ions, this energy loss mechanism competes with the STE to Tl energy transfer. It leads to the characteristic thallium emission, with only one emitting center. This mechanism is described via the constant rate R_1 in our model. It is a linear process as a function of the density of STE. One STE gives one excited Tl that relaxes to emit one photon. These hypotheses are also consistent with the time response presented in Fig.6 and in [34][35]. We mentioned a complex decay curve of NaI:Tl with the presence of an important rise time in the prompt scintillation light and two decay components. The two decay components are ascribed to the two different energy transfer mechanisms, R_1 and R_2, respectively. The prompt one is related to the sequential capture of the electron/hole pairs at a thallium ion. This mechanism is quadratically dependent on the density of electron and hole. The emission takes place when one electron and one hole are both trapped at a thallium site. The delayed energy transfer corresponds to two different processes: the energy transfer from STE's to Tl ions via R_1 and/or the delayed sequential capture of an electron/hole pair at a thallium site. The sequential capture is delayed due to the trapping and release of an electron or a hole from a shallow trap. Neutral and divalent thallium ions are known to be electron and hole traps in NaI, respectively. The rise time shown in the decay is attributed to the delay needed for the STE's to transfer to Tl ions. These hypothesis can also explain the temperature dependence of the NaI:Tl decay curve under gamma excitation published in [34][35]. The delayed energy transfers are highly temperature dependent. At low temperature, the STE to Tl energy transfer and the release of either an electron or hole become slower. This leads to the appearance of the slow component in the decay curve and an increase of its contribution. While the temperature increases the energy transfers become faster. At high temperature, fast and slow components can not be discerned anymore. For intermediate temperature, the delayed transfer is visible in the rise time of the decay curve such as in Fig. 5.

While our simple model fits with good accuracy the response curve, Eq. 9 does not provide a tool to verify all the hypotheses presented above. A more accurate model would imply extensions of our ordinary differential equations. Each energy carrier, STE and electron/hole pairs, would correspond to one differential equation that should then be coupled to simulate the energy transfer between the two different charge carriers. In future work, we intend to treat the more exact case of several energy carrier types.

V. Conclusion

A phenomenological model to study the proportionality response of materials was proposed. The model is based on

the deposited energy density dependence of the scintillation mechanisms. It allows us to describe and explain the electron response of a scintillator in terms of intrinsic properties of the material. The numerical values extracted from the fitting procedure of the model allow us to determine and quantify the main relaxation channels responsible for the non proportionality.

An example was given for the electron response of thallium doped sodium iodide. Based on the analysis, the potential causes of non proportionality were proposed. The non proportional response of NaI:Tl is due to three different mechanisms:

- a linear emission mechanism due to the energy transfer between self trapped excitons and thallium ions.
- a linear quenching mechanism due to the thermal quenching of the STE and/or traps.
- a quadratic emission mechanism due to the sequential capture of an electron/hole pair at a thallium site.
- a cubic quenching mechanism attributed to non radiative auger processes between two electrons and a hole.

The competition between all those mechanisms determines the scintillation response of thallium doped sodium iodide as a function of the deposited energy density. At low density, the emission of NaI:Tl is mainly due to the energy transfer from STE to Tl ions , R_1. The maximum light output can not be reached in this energy range due to the thermal quenching of the STE's, K_1. When the density of charge carriers increases, the second order term R_2 increases. This mechanism is attributed to sequential capture of electron/hole pairs at a Tl site. This mechanism is dominant over the first order term for the electron energies between 10 keV and 1 MeV. The light output increases. At high density, the Auger processes between 2 electrons and a hole leads to an efficient quenching mechanism. The process becomes the dominant one for electron energies inferior to 10 keV. The light output decreases.

Finally, we demonstrated that the combination of accurate electron response data (recorded with SLYNCI apparatus) and model fitting allows a deeper understanding of proportionality in materials. Both provide further insights of the potential causes of non proportionality. In forthcoming works, we plan to further validate our model by studying additional scintillators, developing more accurate scintillation mechanisms by taking into account the case of several energy carriers, and extending the experimental constraint of the fitting procedure by implementing the energy resolution as experimental input in addition to the proportionality response curves.

ACKNOWLEDGMENT

This work was supported by the National Nuclear Security Administration, Office of Defense Nuclear Nonproliferation, Office of Nuclear Nonproliferation Research and Engineering (NA-22) of the U.S. Department of Energy under Contract No. DE-AC03-76SF00098, grant number NNSA LB06-316-PD05 / NN2001000.

REFERENCES

[1] E. V. D. van Loef, P. Dorenbos, C. W. E. van Eijk, K. W. Kramer and H. U. Gudel, Nucl. Instr. & Meth. A, 486 (2002) 254.
[2] N. J. Cherepy, G. Hull, A. D. Drobshoff, S. A. Payne, E. Van Loef, C. M. Wilson, K. S. Shah, U. N. Roy, A. Burger, L. A. Boatner, W. S. Choong and W. W. Moses, Applied Physics Letters, 92 (2008) 083508.
[3] R.B. Murray, A. Meyer, Phys. Rev. B, 122 (1961) 815.
[4] J.E. Jaffre, Nucl. Instr. & Meth. A, 580 (2007) 1378.
[5] P. Dorenbos, J.T.M. De Haas and C.W.E. van Eijke, IEEE Trans. Nucl. Sci., 42 (1995) 2190.
[6] M. Moszynski, Nucl. Instr. & Meth. A, 505 (2003) 101.
[7] M. Moszynski, J. Zalipska, M. Balcerzyk, M. Kapusta, W. Mengeshe, J.D. Valentine, Nucl. Instr. Meth. A, 484 (2002) 259.
[8] D.J. Robbins, J. Electrochem. Soc.: Solid-State Sci. Tech., 127 (1980) 2694.
[9] D.Drouin, A. R. Couture, P. Gauvin, P. Hovington, P. Horney, H. Demers, *Casino MFC Application*, Version 2.42 (2001)
[10] M.Inokuti, Review of Modern Physics 43 (1971) 297.
[11] R.Mayol and F. Salvat, J. Phys. B: At. Mol. Opt. Phys. 23 (1990) 2117.
[12] J.C.Ashley, J. Electron Spectrosc. Relat. Phenom. 28 (1982) 177.
[13] J.C.Ashley, J. Electron Spectrosc. Relat. Phenom. 46 (1988) 199.
[14] D.R.Penn, Phys. Rev. B 35 (1987) 482.
[15] D. E. Cullen, J. H. Hubbell, and L. Kissel, *EPDL97: the Evaluated Photon Data Library, '97 Version, Lawrence Livermore National Laboratory*, UCRL–50400, Vol. 6 (1997) Rev. 5.
[16] G. Bizarri and P. Dorenbos, Phys. Rev. B, 75 (2007) 184302 .
[17] H.B. Dietrich, A.E. Purdy, R.B. Murray and R.T. Williams, Phys.Rev. B, 12 (1973) 5894.
[18] Y. Liu, D. Snoke, Sol. Stat. Comm., 140 (2006) 208.
[19] M. Godlewski, A.J. Zakrzewski, V.Y. Ivanov, J. Alloys Comp., 300-301 (2000) 23.
[20] A. Haug, J. Phys. C: Solid State Phys., 16 (1983) 4159.
[21] A. Zakrzewski, M. Godlewski, Appl. Surf. Sci., 50 (1991) 257.
[22] A. Irreraa, M. Gallic, M. Miritelloa, R. Lo Savioa, F. Iaconad, G. Franza, A. Caninoa, A.M. Piroa, M. Belottic, D. Geracec, A. Politic, M. Liscidinic, M. Patrinic, D. Sanfilippoe, P.G. Fallicae, L.C. Andreanic, F. Priolo, Physica E, in press.
[23] G. Hull et al., IEEE Trans. Nucl. Sci., IEEE Trans. Nucl. Sci. NS-55, June, 2008 (accepted for publication)
[24] W. S. Choong et al., IEEE Trans. Nucl. Sci., IEEE Trans. Nucl. Sci. NS-55 (2008) 1753.
[25] B. D. Rooney and J. D. Valentine, IEEE Trans. Nucl. Sci., 43 (1996) 1271.
[26] S.C. Blankespoor, S.E. Derenzo, W.W. Moses , and C.S. Rossington, IEEE Trans. Nucl. Sci., NS-41 (2004) 698.
[27] S.Kubota, F. Shiraishi, Y. Takami, J. Phys. Soc. Jap., 68

(1998) 291.
[28] T. Huang, W. H. Hamill, J. Phys. Chem. of Solids, 36 (1975) 661.
[29] M. Moszynski, M. Balcerzyk, W. Czarnacki, M. Kapusta, W. Klamra, P. Shotanus, A. Syntfeld, A. Szawlowski, IEEE Trans. Nucl. Sci., 50 (2003) 767.
[30] M. N. Kabler, Phys. Rev., 136 (1964) A1296
[31] R. B. Murray, F. J. Keller, Phys. Rev. 137 (1965) A942.
[32] H. Hitoshi Nishimura, S. Nagata, J. Luminescence., 40&41 (1988) 429.
[33] P. A. Rodnyi, *Physical processes in inorganic scintillators*, CRC Press, NY, (1997)
[34] M. Moszynski, A. Nassalski, A. Syntfeld-Kazuch, T. Szczniak, W. Czarnacki, D. Wolski, G. Pausch, J. Stein, Nucl. Instrum. Meth. A, 567 (2006) 739.
[35] L. Swiderski, M. Moszynski, W. Czarnacki, A. Syntfeld-Kazuch, M. Gierlik, IEEE Trans. Nucl. Sci., 54 (2007) 1372.
[36] M.P.Fontana, W. J. van Sciver, Phys. Rev., 168 (1968) 960.